CHALMERS

Parasitic Component Extraction and EMI Reduction Techniques in an Power Electric Drive System

Master's Thesis in the Master's programme in Electric Power Engineering

HÄRSJÖ, JOACHIM

Department of Energy and environment
Division of Electric Power Engineering
CHALMERS UNIVERSITY OF TECHNOLOGY
Göteborg, Sweden 2011

Parasitic Component Extraction and EMI Reduction Techniques in an Power Electric Drive System

Master's Thesis in the Master's programme in Electric Power Engineering

Master Thesis by:
HÄRSJÖ, JOACHIM

CHALMERS UNIVERSITY OF TECHNOLOGY
Department of Energy and environment
Division of Electric Power Engineering

Financially supported by:
Volvo Car Corp.

Performed during January to June in 2011

Parasitic Component Extraction and Emi Reduction Techniques in Power Electric Drive System

Joachim Härsjö

Examiner: Torbjörn Thiringer

Department of Energy and environment
Division of Electric Power Engineering.
Chalmers University of Technology
SE-412 96 Göteborg
Sweden

Academic Supervisor: Andreas Karvonen

Department of Energy and environment
Division of Electric Power Engineering.
Chalmers University of Technology
SE-412 96 Göteborg
Sweden

Industry Supervisor: Björn Bergqvist

Volvo Car Corporation
Dept. 94820/PV35
SE-405 31 Göteborg
Sweden

Abstract

This thesis focuses on improving the modeling of a filter equipped power electronic drive system model. The filter components are modeled in the FEM calculating software Ansoft Maxwell to see how the component layout affects the component coupling and in extension the EMI performance. After this an EMI-favorable layout was found. The parasitic components of the PCB and the interconnecting cables were computed by implementing 3D models of the circuits, in to the parasitic component extraction software Ansoft Q3D.

It was found that a well chosen placement reduced the coupling factor between the filter inductor and filter capacitors to about $1/3$ in comparison to the most unfavorable placement. Adding the computed parasitic elements to the inverter model resulted in an increase of the simulated EMI of about $20 dB\mu V$ in the entire frequency range. The simulated EMI levels at the multiples of the switching frequency are some $dB\mu V$ lower than the measurement for frequencies lower than $100 kHz$but agrees better in the range from $100 kHz$ to $1 MHz$. At higher frequencies the simulated level is much higher than the measurements.

Key words: *EMI, electric drive system, filter layout analysis, parasitic extraction, PCB modeling, cable modeling*

Acknowledgements

First of all I would like to thank Emanuel Hallgren and Mattias Hedenskog for their cooperation which made this thesis possible together with my supervisor Andreas Karvonen, Ph.D. student at Chalmers, for his help and guidance and for all the fruitful and interesting discussion conducted during this thesis. The guidance from Björn Bergqvist and the financial support from Volvo Car Corp. is grate fully acknowledged. Finally I would like to thank my examiner Prof. Torbjörn Thiringer for his valuable inputs and comments.

Contents

1 Introduction

1.1 General Power Electronic Design and Operation

Prior to the modern computer era, electrical engineers relied on analytical methods when solving electrical related problems. Today, computers are employed to solve complex problems in multiple physical domains. If the objective is to study the electromagnetic interference (EMI) levels in a simulation model of an electric drive system, the electrical engineer has the possibility to use different methods when describing each sub-system (inverter, motor, etc.) of a drive system. In such a scenario, the inverter model consists of functional electrical blocks, including passive components and semiconductor components that are either of system or device level. The outcome of using semiconductor components on device level is that the behavior of the component represents the physical component to a greater extent, compared to a system level component [1].

To obtain accurate EMI levels of a drive system, aside from the parasitic components from the passive components in the inverter, parasitic components due to non-ideal conduction paths in the inverter and parasitic components in the cables must be included in the drive system model design. In addition, the parasitic mutual coupling components in the EMI filter of the inverter and in cable models must be included to provide an accurate model of the drive system where high frequency switching is performed [2], [3].

The EMI filter is a mandatory component in an inverter since EMC standards are becoming more stringent regarding emitted EMI levels. The purpose of the filter is to attenuate outgoing noise generated by the switching devices in the inverter. The design of the filter, i.e. selection of filter components, mainly depends on the wanted cut-off frequency. In reality, the selection of filter components and the layout design of the filter are often determined by the performance in relation to the cost and space available on the printed circuit board (PCB). If a simplified analytical model is used to estimate the EMI filter performance prior to the physical implementation, the filter performance might be degraded since electromagnetic phenomena that occur in the system is not included in the filter calculation model. If the EMI filter is modeled in 3D, with all the physical attributes such as dimensions and material properties taken into account, these

otherwise unforeseen electromagnetic phenomena can be predicted by analyzing the electromagnetic field distribution in the simulation model.

When higher frequencies are considered, the conduction paths and layers of the PCB cannot be seen as ideal since they contribute with stray parasitic components and parasitic coupling components distributed across the PCB. The stray parasitic components consist of self resistances, parasitic capacitance and self inductances that affect the impedance throughout the circuit. The parasitic coupling components provide alternative return paths for the EMI noise. The same modeling approach can be used for cable installations in a hybrid electrical vehicle or in an electrical vehicle where different voltage levels and different cable layouts must co-exist and where EMC standards must be complied. It has been shown in [4] that over-voltages will occur in some drive systems when long cable installations are used in conjunction with high switching frequencies.

Ansys Inc. provides a wide range of simulation suites, covering several fields in the domain of mechanics, fluid dynamics and most importantly, the field of electromagnetics. In particular, Ansoft Simplorer, Ansoft Maxwell and Ansoft Q3D Extractor are of interest where Simplorer serves as the system platform for circuit analysis. Maxwell and Q3D Extractor are used to model a given sub-system such as the EMI filter or the PCB where the results are exported and inserted into Simplorer as a state-space model or an equivalent circuit. Each sub-system in the drive system must be interconnected where the simulation suite is required to exchange solution data between each sub-system.

With the aid of such software, the design of a drive system where each sub-system is modeled on a detailed level is possible. The ability to simulate such a drive system model is important in the branch of electrical engineering, where simulation allows the electrical engineer to predict EMI performance and other functional aspects of a drive system before actually fabricating the prototype. The development cycle thus becomes reduced which results in a lower development cost.

1.2 Problem Description

In [1] a three-phase inverter was constructed and modeled in Ansoft Simplorer. The component models were based on measurements to acquire the correct switching and high frequency behavior. The passive components were measured with an impedance analyzer where the relation between impedance and frequency was studied. The semiconductors, a diode and an IGBT, required more extensive test equipment where special test platforms had to be constructed. The final product of [1] was a fully operational drive system model that was designed with device level components where the drive system model was validated with measurement results.

[1] concluded that there was a mismatch in EMI levels between the simulated drive system model and the physical drive system setup. This indicates that the simulation model of the drive system is partially incomplete due to the idealization of parasitic components that reside within the drive system. Such parasitic components can be the pathways of the PCB or the coupled parasitic components between different components and planes. Traditionally, approximate models are used where the parasitic components are represented with lumped parameters. Today, electromagnetic field simulation software and 3D parasitic extraction software tools are available that can be used to extract parasitic components from the PCB of an inverter and the cabling in the drive system. To study the absolute EMI levels, the parasitic components must be included in the drive system model. In addition, the components in specific parts of the inverter such as the EMI filter can be modeled in the same manner, where different filter layout alternatives may be analyzed before the final implementation.

1.3 Purpose of the Master Thesis

The purpose of this thesis is to model the inverter presented in [1] more in detail in order to capture events of higher frequencies. In this, an important objective is to more in detail account for the circuit layout of the inverter filter by using 3D models of the inductor and capacitor to see the effect of mutual couplings. Another objective is to improve the inverter model presented in [1] with additional parasitic components that originate from non-ideal conduction paths and coupled mechanisms in the inverter. The first aim in improving the inverter modeling is to design a 3D model of the PCB to be able to calculate the parasitic components of it, which then can be added to the inverter model. The second aim is to improve the existing model of the cable sub-system found in [1] with a new model that includes all physical attributes of the cables. A continuously important objective is to measure and compare the EMI performance of the physical drive system and the simulated model.

2 Theory

2.1 Parasitic Components

As shown in [1], passive components cannot be considered as ideal and the same rule also apply for all conductors such as traces, vias and ground planes that provide a current path on the PCB. The non-idealities result in small and often unwanted impedances, called parasitic components that are distributed across the entire PCB. To understand how these parasitic components contribute to EMI in switched environments, definitions regarding the different types of parasitic types are required. The concept of ground must also be revised since the ground cannot be considered as an equipotential surface due to the parasitic components that are present.

Regarding the different types of parasitic components, a distinction must be made between the self parasitic components of a single conductor element and the mutual parasitic components that each conductive element in the PCB has in common.

2.1.1 Self Parasitic Components

Since no ideal conductors exist, each strip, via or plane in the PCB can be represented with a resistive and an inductive part, called the self resistance and the self inductance, shown in Figure 2.1 as R_{self} and L_{self}.

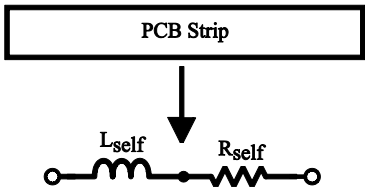

Fig. 2.1: Self parasitics components of a PCB strip.

In the context of self parasitic components, only a single one-directional current carrying element of e.g., a PCB strip is considered where the current return path is not taken into account. As a result, the self parasitic components are often described as the partial self component in order to emphasize that each individual element is a part of a larger current loop. As shown in [1], the magnitude of the

parasitic components within passive components varies with frequency and this also applies for conduction paths in the PCB.

For lower frequencies, the self resistance, $R_{strip,lf}$, of a rectangular-shaped PCB strip can be calculated with

$$R_{strip,lf} = \frac{l}{\sigma w t} \tag{2.1}$$

where l is the length of the strip, σ the conductivity, w the width of the strip and t the thickness of the strip [5]. For cylindrical conductors such as wires and homogenous vias, the resistance, $R_{cylindrical,lf}$ can be calculated with

$$R_{cylindrical,lf} = \frac{l}{\sigma \pi r_w^2} \tag{2.2}$$

where r_w is the radius of the cylindrical conductor. (2.1) and (2.2) apply as long as the criteria $2\delta > t$ is fulfilled where δ is the skin depth which relates to the applied frequency according to

$$\delta = \frac{1}{\sqrt{\pi f \mu_0 \sigma}} = \frac{6.6*10^{-2}}{\sqrt{f}}. \tag{2.3}$$

For higher frequencies where $2\delta < t$, the self resistance, $R_{strip,hf}$, of a rectangular strip can be calculated as

$$R_{strip,hf} = \frac{1}{2\sigma\delta(w+t)} \tag{2.4}$$

and the resistance of a cylindrical conductor, $R_{cylindrical,hf}$ can be calculated as

$$R_{wire,hf} = \frac{1}{2\sigma\pi r_w \delta}. \tag{2.5}$$

It can be seen from (2.4) and (2.5) that the self resistance increases with increasing frequency as expected due to the skin effect. It can also be seen that the self resistive parasitic component is reduced by increasing the cross-section of the conductor, as well as keeping the conductors short.

When the self inductance of a conductor, such as a PCB strip or a via, is calculated, approximate calculation models are often used. The self inductance, $L_{strip,lf}$, of a rectangular PCB strip can according to [6] be approximated with

$$L_{strip,lf} = \frac{0.002l\left[ln\left(\frac{2l}{w+t}\right) + 0.5 + 0.2235\left(\frac{w+t}{l}\right)\right]}{10^6} \quad (2.6)$$

where l, w, t are the length, width and thickness of the PCB strip, respectively. It can be seen in (2.6) that the relation between the width/thickness and the length is important to keep the self inductance minimum. The self inductance of a generic conductor or wire is in the order of $5 - 10\ nH/cm$ [5].

2.1.2 Mutual Parasitic Components

Between each trace, via and plane on the PCB or between different electrical devices in a drive system, electromagnetic coupling, will occur due to the mutual parasitic components that are present in the system. This is usually referred to as crosstalk and the general principle is that electromagnetic energy, is unintentionally transferred from one conductor to another via electromagnetic fields. In the context of EMC, the conductor that emits the energy is often called source while the recipient conductor is called the victim. There are three types of coupling mechanisms: common impedance coupling, capacitive coupling and inductive coupling. Technically, capacitive and inductive coupling fall under the category of common impedance coupling but in this case, common impedance coupling is referred to the conductive connection between two conductors while the capacitive and inductive coupling are due to induction by electromagnetic fields.

Common impedance coupling occurs when two or several circuits share a common impedance to ground as shown in Figure 2.2 where the return path of Circuit B is connected to Circuit A. The ground plane cannot be considered as an equipotential surface with zero impedance due to the parasitic components which are represented as the self impedances Z_A and Z_B.

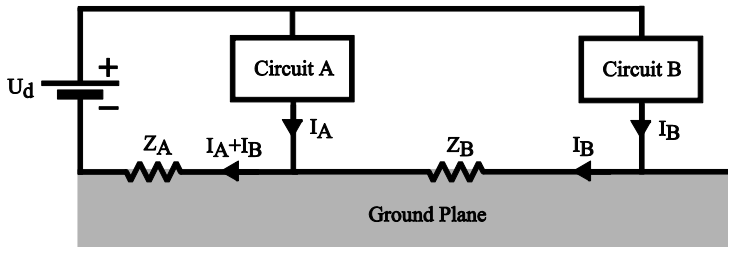

Fig. 2.2: Common impedance coupling between two circuits.

In this case, the current signature that creates a voltage drop over Z_B depends on I_B and the voltage drop over Z_A is determined by the sum of $I_A + I_B$. The current, I_B from Circuit B will thus superimpose on the return path of Circuit A which

results in that the potential at the ground point, $V_{gnd,A}$ of Circuit A will vary with the current from Circuit B. The same is applicable for the other way around where the potential at the ground point of Circuit B is $V_{gnd,B} = Z_A I_A + (Z_A + Z_B) I_B$ [5].

Inductive coupling is a phenomenon that occurs between two conductors where one of the conductors (source) subjects another conductor (victim) with a time-varying magnetic field. The varying current, $i_{source}(t)$, in the source conductor will thus couple with the victim conductor via the magnetic flux in a path that is represented by a parasitic mutual inductance L_m, see Figure 2.3.

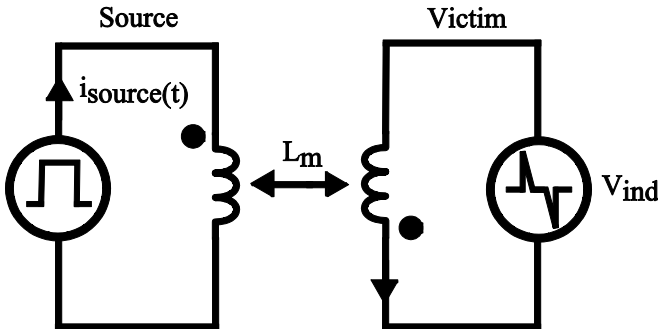

Fig. 2.3: Inductive coupling between two conductors.

The induced voltage on the victim conductor is

$$V_{ind} = -L_m \frac{di_{source}(t)}{dt} \tag{2.7}$$

where L_m is mutual inductance the between the conductors. From (2.7), it can be concluded that high current transients will result in high inducted voltages on adjacent conductors. The magnitude of L_m depends on the coupling factor k and the self inductances of each cable, such as

$$L_m = k\sqrt{L_{self,source} L_{self,victim}} \tag{2.8}$$

where $L_{self,source}$ and $L_{self,victim}$ are the self inductances for the source and victim conductor, respectively. The coupling factor is a value between 0 and 1 where a value of 1 indicate maximum inductive coupling between two conductors. Inductive mutual coupling is widely used in AC transformer applications where two wires are winded around the same magnetic core to transform a voltage. In a case where the magnetic leakage flux is minimal, the coupling factor is almost 1. The magnitude of the coupling factor further depends on the length of each conductor as well as the distance between each conductor. The mutual inductance between two rectangular PCB strips, can be calculated as

$$L_m = \frac{0.002l\left[ln\left(\frac{2l}{d}\right) - 1 + \left(\frac{d}{l}\right)\right]}{10^6} \qquad (2.9)$$

where l is the length of the strip and d the distance between each conductor [6].

The capacitive coupling phenomena occur between conduction paths and planes of the PCB where time-varying electrical fields exist. The electrical field between e.g., two conductors is due to a difference in voltage potential and it is the mutual parasitic capacitance, C_m, between the two conductors that provide a path for EMI. Figure 2.4 shows a circuit where C_v and R_v is the capacitance and load resistance of the victim circuit. In a similar manner as for inductive coupling, between two conductors, one conductor is often defined as the source and the other conductor as victim.

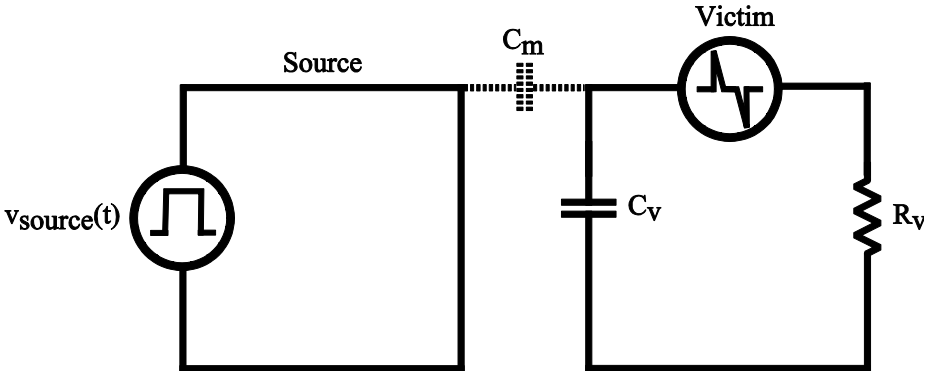

Fig. 2.4: Capacitive coupling between two conductors.

According to [7], the magnitude of the voltage noise that is induced on the victim conductor depends on the frequency of $v_{source}(t)$ and C_m. The induced noise voltage can be calculated with

$$v_{ind}(t) = j\omega R_v C_m v_{source}(t) \qquad R_v \ll \frac{1}{j\omega(C_v + C_m)} \qquad (2.10)$$

and

$$v_{ind}(t) = \left(\frac{C_m}{C_m + C_v}\right) v_{source}(t) \qquad R_v \gg \frac{1}{j\omega(C_v + C_m)} \qquad (2.11)$$

The mutual capacitance between two parallel conductors can be defined as

$$C_m = \frac{27.6l\varepsilon_{r(eff)}}{10^{12}\ln\left(\frac{d}{r_w} + \sqrt{1 - \left(\frac{2r}{d}\right)^2}\right)} \qquad (2.12)$$

where d is the center distance between the conductors, r_w is the wire radius, l is the length of the cables and $\varepsilon_{r(eff)}$ is the effective permittivity [7]. The impact of capacitive coupling can thus be decreased by reducing the frequency in the application, decrease the parallel length, increase the distance between the conductors, increase C_r, decrease R_v, or by shielding the objects.

2.2 EMI

EMI has become a common phenomenon in modern power electronics as of today where switching power supplies are utilized. A brief history and general principles regarding, how EMI is defined and how it can be measured is covered in [1]. The same measuring approach is used throughout this master thesis, except for an EMI noise separator device that is introduced in section 3.2.2.

In an inverter where power transistors such as MOSFETs and IGBTs are used, EMI is imminent due to fast transitions of voltages and currents. The generated noise level depends on factors such as the switching scheme of the IGBTs, driving techniques, parasitic components, gate resistances, etc. As diodes are often used for free-wheeling purposes in such applications, they also contribute to the total EMI due to reverse recovery.

It has been previously stated that parasitic components from non-ideal passive components and non-ideal PCB conduction paths will contribute to the total EMI in the system where the behavior of these components are far from ideal. In [1], it was shown how the impedance of passive components such as resistors, capacitors and inductors vary with the frequency. However, it was not presented how the parasitic components couple and affect the EMI performance of a drive system. It can be concluded that, in order to improve the EMC and reduce EMI phenomena in a drive system, different sources of EMI and the propagation paths have to be studied to a greater extent.

2.2.1 Sources and the Concept of CM/DM Noise

There are several potential EMI sources in an electrical circuit. Since the most effective way to reduce EMI in a system is to limit the contributing noise at the source, each EMI source in the system has to be recognized and dealt with. Generally, a distinction can be made between sources that actually generate EMI due to functionality such as power switching devices and EMI sources which contribute to the EMI due to non-ideal behavior. These effects have to be taken into account during the design process of the PCB where the layout of the conduction paths and the component placement is done.

The total conducted EMI noise consists of two components: common-mode (CM) noise and differential-mode (DM) noise [5]. In order to quantify these two components, one can say that CM noise propagates between each conductor with

respect to ground through parasitic components, while DM noise propagates between conductors [8], see Figure *2.5*.

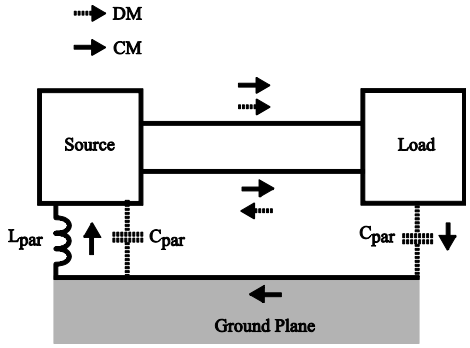

Fig. 2.5: CM and DM propagation paths between a source and load.

The magnitude of the two components will differ from each other and the magnitude of each component will also vary with frequency. Due to this, one component might be dominant in one frequency range, while the other component might be dominant in another frequency range. In [5], it is stated that the largest contributor to the total conducted EMI is the CM noise component. A distinction between how CM and DM noise are generated and how these noise modes propagate is critical if the goal is to study and reduce EMI phenomena in a drive system.

2.2.2 Common-Mode Noise

CM noise is mainly generated by the switching behavior of semiconductor devices such as IGBTs and diodes that have high voltage slew rates. Due to the switching, the voltage on each connection point in an inverter will vary with respect to ground, given that they are not directly connected to ground. As a result, there will be a parasitic capacitance between the connection point and ground that provide a travel path for CM currents where the CM current will return to the power source, as shown in Figure 2.5.

A large contributor of CM noise in an inverter is the parasitic capacitances that are present between the semiconductor devices and the mounted heat sinks. Between the back plate of the device and the heat sink there is a thin electrical insulating layer where the heat sink is normally grounded for safety. Since the two electrodes will have different potentials, the electrical insulating layer will act as a dielectric layer and thus a parasitic capacitance, $C_{heatsink}$ between the device and ground will appear and act as a noise leakage path, as shown in Figure 2.6.

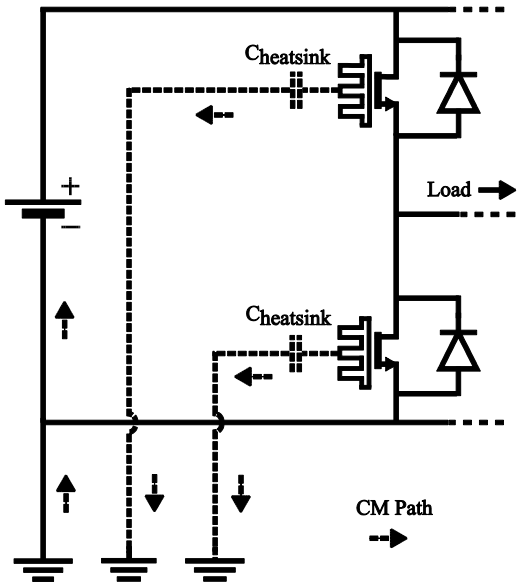

Fig. 2.6: CM propagation path from grounded heatsink to source.

The value of the capacitance depends on the material characteristics of the insulation layer. This capacitance will further be charged and discharged during the on- and off-transitions of the device, which will result in a CM current that will propagate through the ground loop back to the power source. The magnitude of the CM current is stated as

$$i_{CM} = C_{heatsink} \frac{dv}{dt} \tag{2.13}$$

where $C_{heatsink}$ is the parasitic capacitance and $\frac{dv}{dt}$ is the voltage slew rate of the semiconductor devices.

In a drive system, CM currents may also appear between the inverter and motor, where the CM currents also will find a propagation path from parasitic capacitances that are present between the cable windings and ground. The CM currents can be controlled or limited in various ways by reducing the stray capacitances between the CM source and ground or by adding CM filters.

2.2.3 Differential-Mode Noise

DM noise is present in the system due to the switching behavior of the semiconductor devices. Compared to CM noise caused by electrical couplings, DM noise is caused by magnetic couplings in a current loop that includes parasitic inductances where the current loop is being subjected to a high current slew rate. The DM noise voltage source can be stated as

$$v_{DM} = L_{loop,parasitic} \frac{di}{dt} \tag{2.14}$$

where $L_{loop,parasitic}$ is the current loop inductance and $\frac{di}{dt}$ is the current slew rate generated by the semiconductor device.

As the DM noise propagates in opposite direction from the source to load, as shown in Figure 2.5, there will be voltage differences on the DC-bus of the inverter due to the stray parasitic components [9]. Aside from this, the capacitors on the input stage of the inverter will also be subjected to the high current derivative that is created by the switching of the IGBT and diodes and thus there will be a voltage drop over the equivalent series resistances of the capacitors. In scenarios where bulky energy reservoir capacitors with high equivalent series resistances are used, this effect will be even more evident.

There are several ways to suppress DM noise in a system. One important aspect is the layout design of the PCB, where the current loop areas should be as small as possible to keep the loop inductance small. Also, devices that are noise sensitive should be kept apart from sources of high current switching. Bypass capacitors are also traditionally installed in the vicinity of the DM source where the bypass capacitor presents an alternative return path to the pulsating current.

2.2.4 Separating CM and DM noise

It was stated above that the total EMI on the input stage of the inverter has to be separated into two noise modes, CM and DM, where the separation can be done in at least two ways.

One solution is to separate the noise modes directly in the measuring equipment such as an oscilloscope. This can be done if the oscilloscope has more than two input channels where the oscilloscope must be capable of performing algebraic calculations on the obtained signals in the time-domain. If $v_{LISN(pos)}$ is defined as the measured voltage on the positive LISN port, and $v_{LISN(neg)}$ is defined as the measured voltage on the negative LISN port, the analogue noise quantities, v_{CM} and v_{DM}, can be expressed as

$$v_{CM} = \frac{v_{LISN(pos)} + v_{LISN(neg)}}{2} \tag{2.15}$$

and

$$v_{DM} = \frac{v_{LISN(pos)} - v_{LISN(neg)}}{2} \tag{2.16}$$

where naturally $v_{LISN(pos)}$ and $v_{LISN(neg)}$ both contain CM as well as DM noise. These two quantities further need to be translated from time-domain to frequency-domain by applying the Fast Fourier Transform (FFT).

An alternative way to separate these noise modes is to build a noise separator which may be constructed in various ways. The general principle of the noise separator is that it rejects DM noise in one current path while it rejects CM noise in another current path, and thus each noise signal can be measured separately by an oscilloscope or spectrum analyzer.

2.3 Q3D Parasitic Component Extraction

It is important to take parasitic components and non-ideal conduction paths into account when the objective is to model a drive system with emphasis on EMI performance. A common method to introduce parasitic components into a model is to use approximate equations to calculate the parasitic resistance of a PCB trace as shown in (2.4) where lumped parameters are used to represent a PCB trace. This method becomes highly time consuming as the complexity of the structure increases and the coupling factors becomes more dominant making the method less useful.

An alternative method to extract the parasitic components and coupling factors is to use the software Q3D Extractor which calculates parasitic components such as the stray capacitance (C), conductance (G), resistance (R) and inductance (L) in both 2D and 3D structures for frequencies up to 1.5 GHz [10]. These parasitic components can be calculated on CAD-models which can be created in Q3D or be imported from external software suites such as Pro Eng or AutoCAD.

Q3D Extractor utilizes two methods to calculate the self parasitic and mutual parasitic components of a structure; Method of Moments (MoM) and Finite Element Method (FEM). Which solver method used depends on which entities will be solved which Q3D has divided into three sub parts; capacitance and conductance, DC resistance and inductance and AC resistance and inductance. MoM is used in almost all calculations where it uses the approximated surface charge density. FEM is only used for calculating the DC resistance via current volume density.

For Q3D to be able to solve an electrostatic setup to calculate the capacitive and conductance properties of a model, each conducting body in the model has to be assigned to a net which Q3D then uses when it creates surface meshes on all the conductors and dielectrics. These defined nets will then be used in the calculation of all the parasitic components. The capacitances between separated nets are calculated with the separating material taken into account. To solve the conductance part of the problem, Q3D excites on one net with one volt at a time, i.e. the other nets are set to zero volt. The distribution of free charges within each

net along with the bound charges on the dielectric surfaces is then calculated. The charges are restricted by certain boundary conditions which are summed up for each conductor resulting in a matrix containing the charge relations between each defined net. With a known charge relation, Q, the capacitance and conductance can be calculated with

$$(G + j\omega C)V = j\omega Q \tag{2.17}$$

where the real part is the conductance, G, and the imaginary part is the capacitance, C [10]. To solve a magnetostatic setup, which calculated the resistance and inductance, each conductor has to have an assigned sink and at least one source to define the current path. The solution procedure for solving a magnetostatic setup is similar to the electrostatic setup, but instead a current excitation is used. One ampere is applied at a time in one source where the sources are not connected. The parameter is then extracted by calculating the current density in each conductor.

Independent of solution setup, the calculated results are presented in a square matrix where all the self- and mutual values are presented. In the result matrix, the self values are presented in the diagonal row, whereas the mutual values are presented in the off-diagonal row. Note that the terms self value and mutual value are used in a general sense and the actual value depends on the setup. In Figure 2.7 two conductors are shown where the left conductor includes two separate parallel sources (Source 1 and Source 2) which are joined together to a common source (Sink 1). In this case, the self resistances are denoted as R_{11}, R_{22} and R_{33} while the mutual resistance between Source 1 and Source 1 is R_{12}, which is equal to R_{21}.

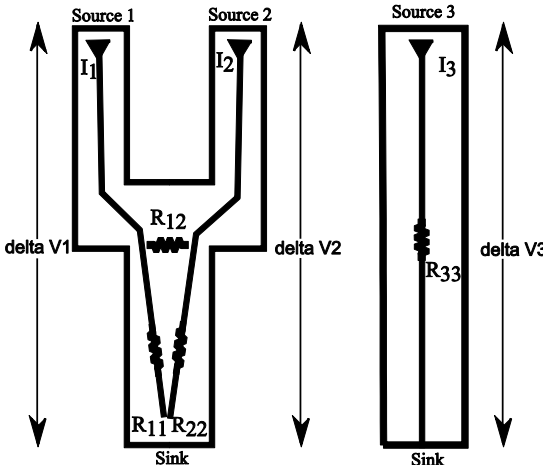

Fig. 2.7: Two conductors illustrating the concept of self resistance and mutual resistance.

To extract the resistive components in a setup as shown in Figure 2.7, Q3D uses a Laplace function to calculate the volume current in the design, where resistance matrix can be described as

$$\left(\nabla V_{1,2,3}\right) = \begin{pmatrix} R_{11} & R_{12} & 0 \\ R_{21} & R_{22} & 0 \\ 0 & 0 & R_{33} \end{pmatrix} \left(I_{1,2,3}\right) \tag{2.18}$$

The calculated entities can be extracted as matrices or the solved model can be used in a Simporer co-simulation, or it can be exported as a state-space model which also can be used in Simplorer. If the state-space model is applied, it is possible to pre solve the problem setup for a given frequency range. By using co-simulation with Simplorer the accuracy increases as Simplorer specifies the current frequency and currents to Q3D but at a cost of increase in calculation time.

3 EMI Filter Synthesis

3.1 Modeling of Filter Components

In [1], equivalent models were used to represent the frequency behavior of the passive components in the EMI filter which consists of two plastic film capacitors connected in parallel on each side of an inductor in series with the DC voltage input, see Figure 3.1.

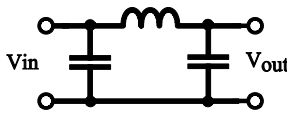

Fig. 3.1: Two parallel capacitors connected to an inductor in series, forming a low-pass EMI filter.

With this approach, the self parasitic components of EMI filter are accounted for but not the mutual couplings or the PCB. The mutual couplings between each passive component in the EMI filter was not included in the equivalent models due to the complex structure where coarse approximations had to be used to calculate the mutual parasitic components. Another approach to extract the mutual parasitic components from the EMI filter is to create a CAD-model of each component where the FEM is used to calculate the electromagnetic fields in the vicinity. Material properties and physical dimensions of each component are included in the CAD-model.

FEM calculations require a lot of computational resources and are therefore time consuming for highly detailed models. If the model is too detailed, the FEM software might not be able to converge which results in an unsolvable setup. As a result, simplifications are often made in the modeling process. In this thesis a hybrid solution is introduced to analyze the impact of the mutual parasitic components in the EMI filter. The hybrid solution combines the equivalent models from [1] with the extracted mutual parasitic coupling components from the CAD-model. Each CAD-model is designed according to the outer dimensions of the component where the internal material and dimensions are altered to obtain the correct properties. Maxwell is used through the whole analysis, from the initial modeling stage where the component are modeled and material properties are set, to the solving stage where FEM calculations are performed and analyzed.

3.1.1 Plastic Film Capacitor

The internal structure of the plastic film capacitor is reduced from a rolled up plastic film to an E-shaped structure. In the CAD-model both the conductive part of aluminum and the dielectric part are enlarged, compared to a physical capacitor. The curled up plastic film of the physical capacitor has an elliptical shape which is embedded in a rectangular plastic casing. The E-shaped structure run vertically from the connector pins forming a box, shaped as a rectangle according to the outer dimensions of the physical capacitor, see Figure 3.2.

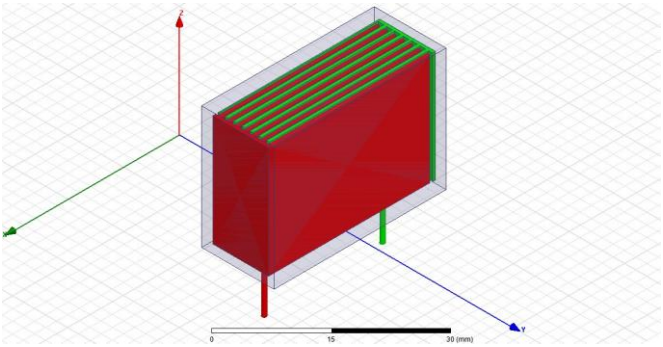

Fig. 3.2: Plastic film capacitor CAD-model.

In Maxwell the electrodes of the capacitor are assigned as aluminum which has a pre-defined conductivity. The set of electrodes are enclosed with a dielectric material that serves as dielectric between the electrodes as well as the casing of the capacitor.

To calculate the capacitance of the capacitor model the electrostatic solver is used where one electrode pin is excited to $1V$ and the other electrode pin is set to $0V$. As the calculated capacitance between two voltage exited electrodes depends on the permittivity of the dielectric between the electrodes, the relative permittivity has to be altered to obtain the same capacitance value as the real capacitor. The extreme value of the relative permittivity is due to the simplification made in the inner parts of the capacitor where the area between the electrode sheets are vastly larger compared to the modeled capacitor. The electrical potential on a cross section of the solved capacitor model is shown in Figure 3.3.

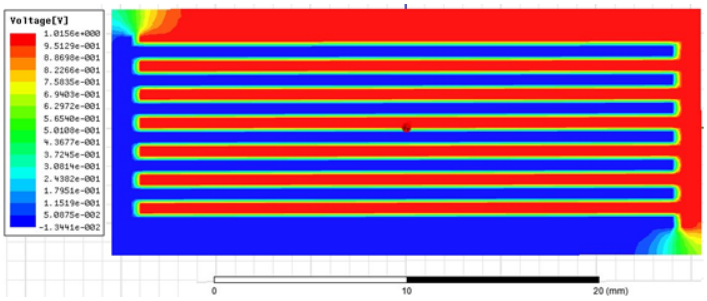

Fig. 3.3: The electric potential on a cross section of the solved capacitor, seen from above.

Since the electrostatic solver calculates the capacitance between all excited nodes, it also calculates the capacitive coupling coefficient between different components. The coupling coefficient between two capacitors separated by a distance of about $7mm$ (casing to casing) is calculated to $k = 5 * 10^{-10}$, i.e., the parasitic coupling capacitor is about $0.5pF$ which will only affect frequencies above the GHz region. Since the frequency range of interest in this thesis is up to $30MHz$ the capacitive couplings are neglected. The small coupling capacitance indicates that the fictional value of the relative permittivity will not introduce an error in the EMI filter analysis that includes the inductive couplings.

The electrolytic capacitors will not be modeled because of their complex inner shape and since they are placed far away from the inductor and which makes the coupling factor negligible, see section 3.2 for further analysis.

3.1.2 Inductor

The inductor consists of copper wires which are wound around a bobbin core with 106 turns, the CAD-model of the inductor is shown in Figure 3.4. The inductor core is set to ferrite where the winding is set as copper, where the material properties used is from Maxwell's material library.

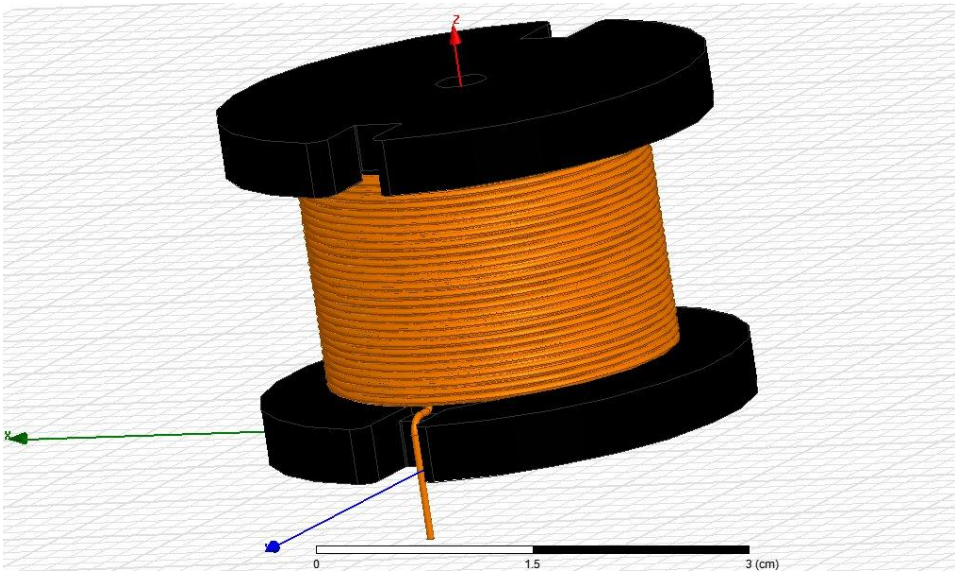

Fig. 3.4: Detailed bobbin core inductor CAD-model.

The detailed CAD-model of the inductor, shown in 3.4, is too complex for Maxwell to mesh and solve within reasonable a time. A simplified CAD-model is therefore made, with an identical core as the previous model but the numbers of

turns are greatly reduced and the cross section of the wiring is changed from circular to square, see Figure 3.5.

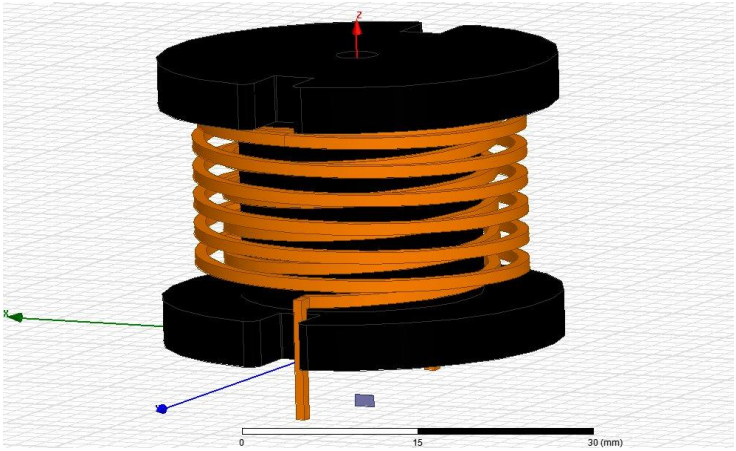

Fig. 3.5: Simplified bobbin core inductor CAD-model.

The inductor model is solved using both the magnetostatic solver as well as the eddy current solver which solves the eddy currents in a structure for different frequencies. In both solutions, the wiring is excited with a current of $1A$. The magnetostatic solution shows that magnetic field is not contained within the core as some field leaves the core; see Figure *3.6* where the magnetic field is depicted as streamlines in the YZ-plane. As expected, the magnetic field is stronger closer to the core, where it decreases with distance from the core, i.e., objects close to the coil will be more affected by the leakage flux.

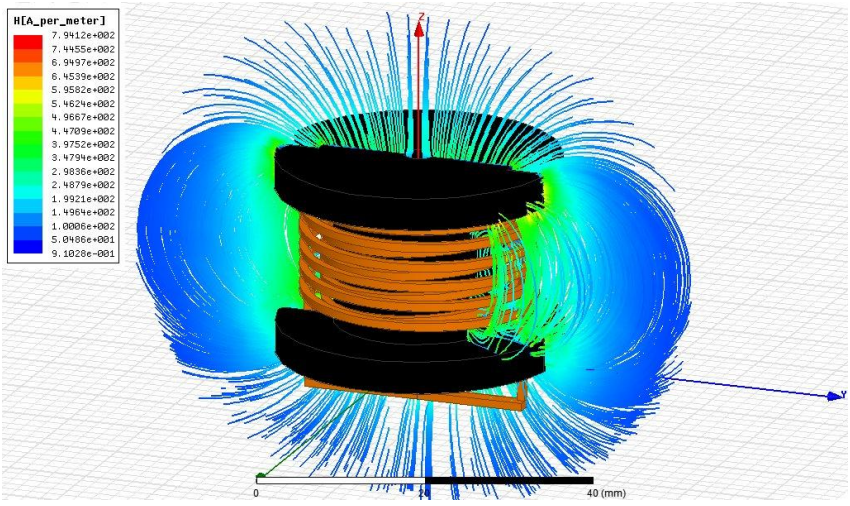

Fig. 3.6: Magnetostatic solution showing the H-field as streamlines.

The inductance value of the reduced inductor model is found to be much less compared to the values given in the datasheet. The inductor model cannot be altered to obtain the correct inductance, as for the plastic film capacitor. Instead a post-processing option is used which allows the user to alter obtained simulation results. With the post-processing option, one winding turn in the CAD-model can be set to represent several winding turns after post-processing, i.e., the number of winding turns can re-specified once results from the CAD-model are obtained. This feature is however only available for magnetostatic solutions.

The magnetostatic solver as well as the eddy current solver can be used to calculate inductive couplings and thus extract the mutual parasitic components between different components in the EMI filter. At least two current excitations are required to solve the inductive couplings between the modeled components since Maxwell calculates the interaction of the magnetic fields generated by each current.

One drawback of Maxwell is its inability to solve an electrostatic and magnetostatic model simultaneously, i.e., the capacitive and the inductive coupling must be solved separately since the interaction of these two coupling mechanisms cannot be simulated.

3.2 Filter Layout Analysis

It is important to include the self and mutual parasitic components which reside in an EMI filter in the simulation model since the filter components spread electrical or magnetic fields in its vicinity to a large extent. The component placement affects the mutual coupling between the EMI filter components and by extension, the overall filter performance. The DM noise level can be reduced by optimum component placement [11].

3.2.1 Simulation

The first component configuration layout consists of the simple inductor that was modeled in section 3.1.2 and the capacitor modeled in section 3.1.1, see Figure 3.7. The inductive coupling between each component is found using the magnetostatic solver which only accepts current excitations and not voltage excitations. Since a voltage cannot be applied over the capacitor and the dielectric is an insulator, the capacitor model is altered so that electrodes on the capacitor are connected with an additional highly resistive connector pin. This approach enables a current excitation of $1\mu A$ through the capacitor where the inductor current set to $1A$.

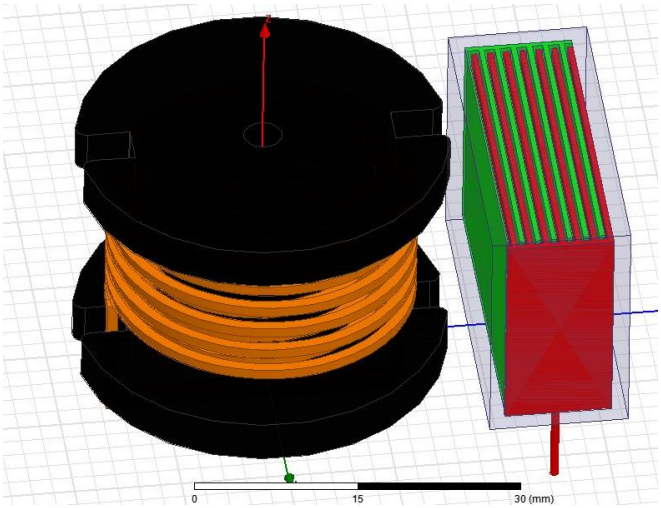

Fig. 3.7: Component configuration layout of the inductor in proximity to the plastic film capacitor.

The mutual inductive coupling between these components is calculated to $L_m = 0.423\mu H$. The coupling factor is calculated to $k = 53 * 10^{-3}$ if the self inductance of the inductor is used as reference. The coupling factor is used throughout the filter layout analysis to express the magnitude of inductive coupling where the coupling factor is always expressed as relative to the self inductance, which makes the post-processing option superfluous.

Figure 3.8 shows the calculated coupling factor for different distances between two inductors and between an inductor and a capacitor. The distance is defined as the shortest distance between the capacitor casing and the inductor core or the core to core to distance. The simulation results indicate that an increase of the distance between components radically reduces the coupling factor.

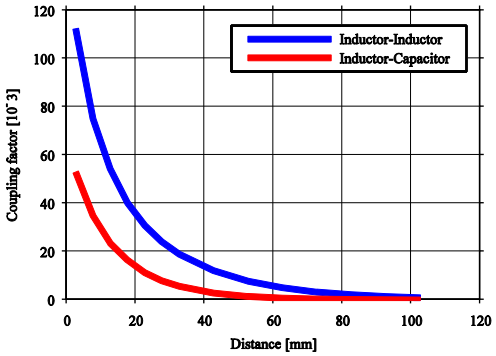

Fig. 3.8: Component configuration layout of the inductor in proximity to the plastic film capacitor.

When the eddy current solver is used, the frequency of the exited current is varied which gives the possibility to study the frequency dependence of both the self inductance together with the inductive coupling between the inductor and the capacitor. Table 3.1 shows the simulated results of how the coupling coefficient changes with current frequency.

Table 3.1: The inductive coupling factor for different frequencies of the current.

Frequency [Hz]	0.1	1	100	1000	5000	10^4	10^5	10^6	10^7
k [10^{-3}]	53.3	53.3	53.0	47.8	44.6	44.0	44.0	45.2	45.4

The simulation results show that the inductive coupling is stronger for lower frequencies and above $5kHz$ the inductive coupling becomes almost independent to the frequency. This facilitates the modeling since the coupling can be modeled as a static coupling.

The inductive coupling does not only depend on the distance and the frequency, but on the component placement as well. According to [11] the filter performance can be improved by aligning the filter components in various ways to reduce the coupling factor. To verify this, two different filter layouts are modeled according to the filter schematic in Figure 3.1. The simplified inductor from section 3.1.2 and the capacitor modeled in section 3.1.1 are used in the modeling process. The difference between each filter layout is the alignment of the capacitors. In the first layout, shown in Figure 3.9, the capacitors are placed in parallel with the inductor and in the second layout, the capacitors are rotated 90° in comparison to the capacitors in the first layout, see Figure 3.10.

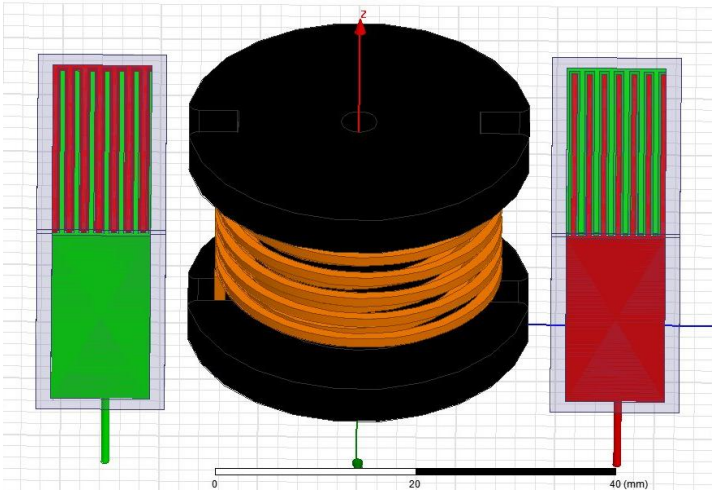

Fig. 3.9: First filter layout with the capacitors in parallel with the inductor.

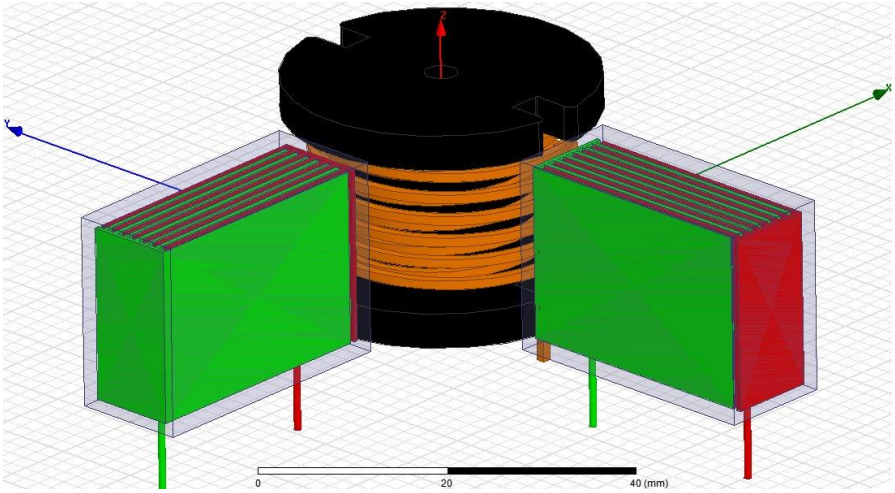

Fig. 3.10: Second filter layout where the capacitors are rotated with 90°.

The magnetostatic solver is used to solve both filter layout models where the inductor is excited with $1A$ of current and the capacitors are excited with $1\mu A$ of current. The calculated coupling factor between the inductor and each of the capacitors for each filter layout model is shown in Table 3.2.

Table 3.2: Coupling factors between the inductor and the capacitors for each filter layout model.

	k between first capacitor and the inductor [10^{-3}]	k between second capacitor and the inductor [10^{-3}]
First filter layout	54.3	54.0
Second filter layout	18.6	19.5

The simulation results indicates that the first filter layout where the capacitors are aligned parallel with the inductor has a lower coupling factor and is thus favorable from an EMI perspective. The results also verify that the distance between each filter component may be reduced without an increase in the inductive coupling, as long as the filter components are aligned optimally. The results also agree with the conclusions made in [11] where it is stated that the first filter layout gives better EMI performance compared to the second filter layout.

By adding the mutual coupling to the filter derived in [1] between the main inductor and a parasitic inductor in the capacitor the filter performance changes. Figure 3.11 shows the coupling effect on the filter transfer function in comparison without any coupling.

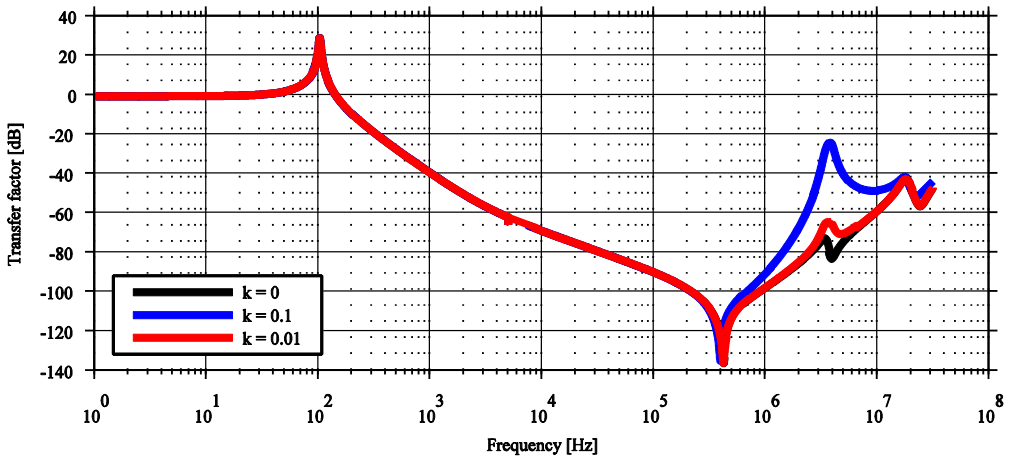

Fig. 3.11: Comparison of filter with different coupling factors

The addition of mutual coupling, calculated in Maxwell, has almost no impact on the filter performance due to the small coupling factor. The only noticeably difference appears close to $4MHz$, see Figure 3.12.

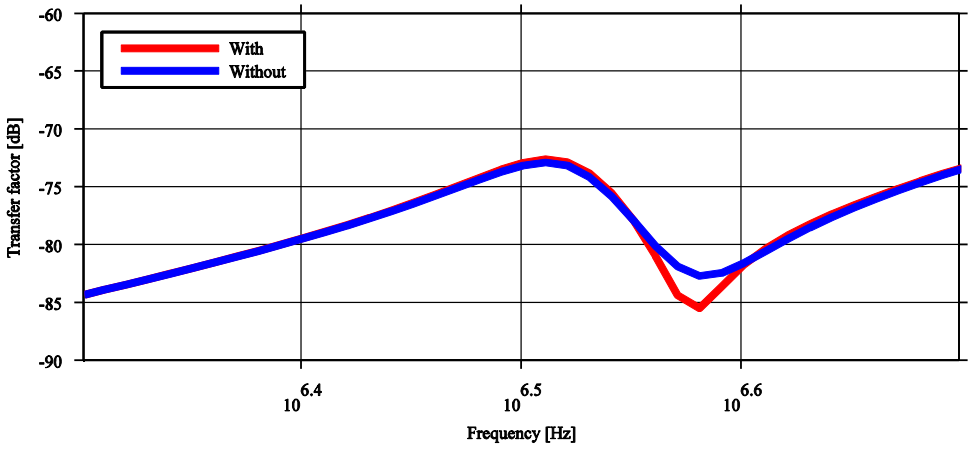

Fig. 3.12: Effect of Maxwell calculated coupling

This shows that the accurate coupling is difficult to model but the simulation results are still useful since it verifies the principles of how different layouts affects component coupling.

3.2.2 Measurements and Validation

To validate the simulation results, each filter layout is constructed and connected to the inverter one at a time where the EMI on the input stage of the inverter is measured. The measurement setup consists, of two LISN devices that are

connected on the positive and negative DC link, between the DC voltage input and the EMI filter. The ground consists of a grounded copper plate where the inverter and the LISN devices are placed on the same ground plate. The spectrum analyzer (Hewlett Packard 8591EM EMC analyzer) that is used during the measurement is not capable of separating the CM and the DM component from the measured noise components on the LISN devices. Due to this, a noise separator is constructed to separate the CM and DM noise [12]. A simplified schematic of the measurement setup is depicted in Figure 3.13.

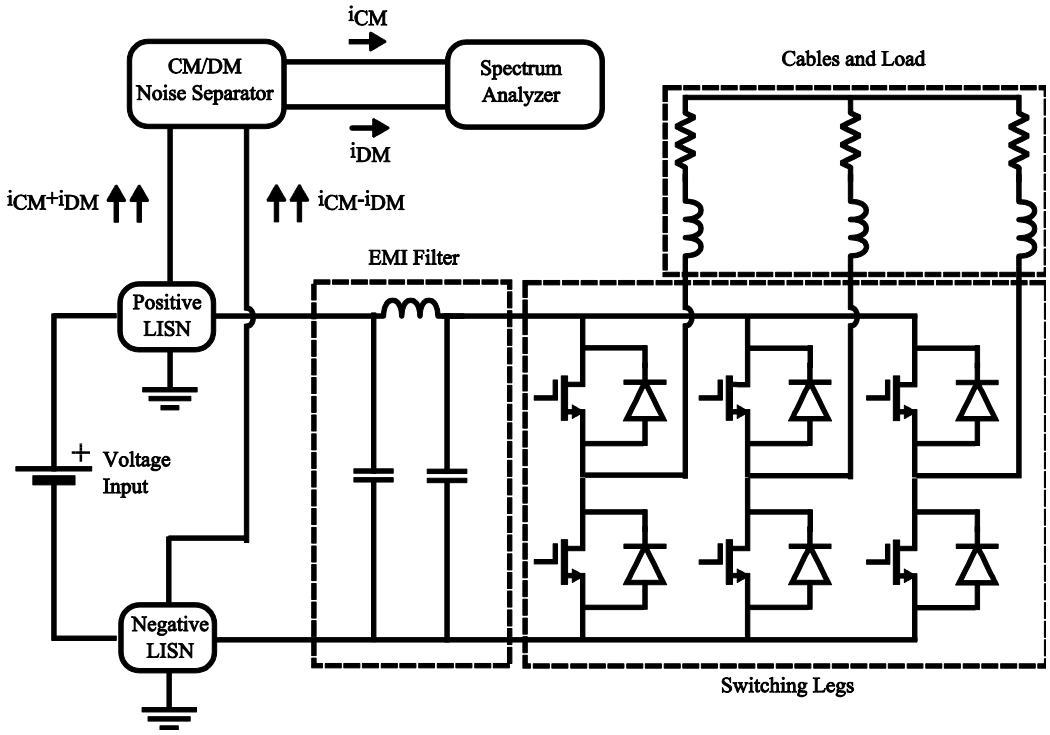

Fig. 3.13: Simplified schematic of the measurement setup.

The separator consists of two high precision 50Ω resistors, a wideband transformer and a ferrite toroid. The primary transformer is the main component that distinguishes the DM noise from the CM noise since only the DM noise is transformed to the secondary side. The CM noise is canceled out in the transformer on the primary side since the CM traveling path has the same direction, i.e., the noise currents into both the positive and negative LISN device has the same direction. The DM noise does not travel in the same direction and is therefore transformed to the secondary side of the transformer, see Figure 3.14. The resistors on the CM and DM outputs act as measuring terminators where the CM noise is picked up over the resistor R_{CM} and the DM noise is picked up over the resistance R_{DM}. It is important that the transformer does not damp the incoming noise for the frequency range of interest. The power rating on the transformer can however be low since the noise power levels are low. The ferrite

toroid on the secondary side of the transformer acts as a CM-choke where it reduces non-wanted CM noise on the secondary side.

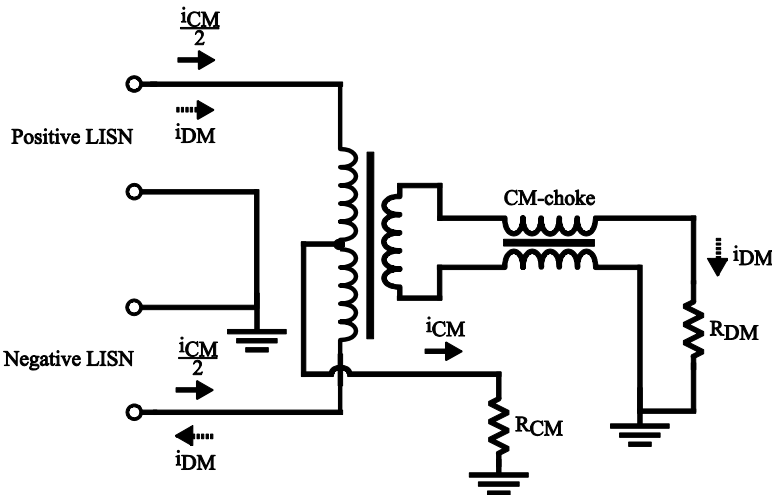

Fig. 3.14: The CM and DM noise separator setup.

During the measurement, the inverter operates at a switching frequency of $20kHz$ and a fundamental frequency of $70Hz$. The inverter is fed with $300V$ from a DC power supply (Elektra $300V$, $20A$) and the inverter is loaded with an asynchronous machine. The DC power supply deliver $1.1A$ i.e., $330W$ during the measurement. Figure 3.15 show the measured DM noise for both the filter layout with the optimal capacitor placement and the unfavorable capacitor placement.

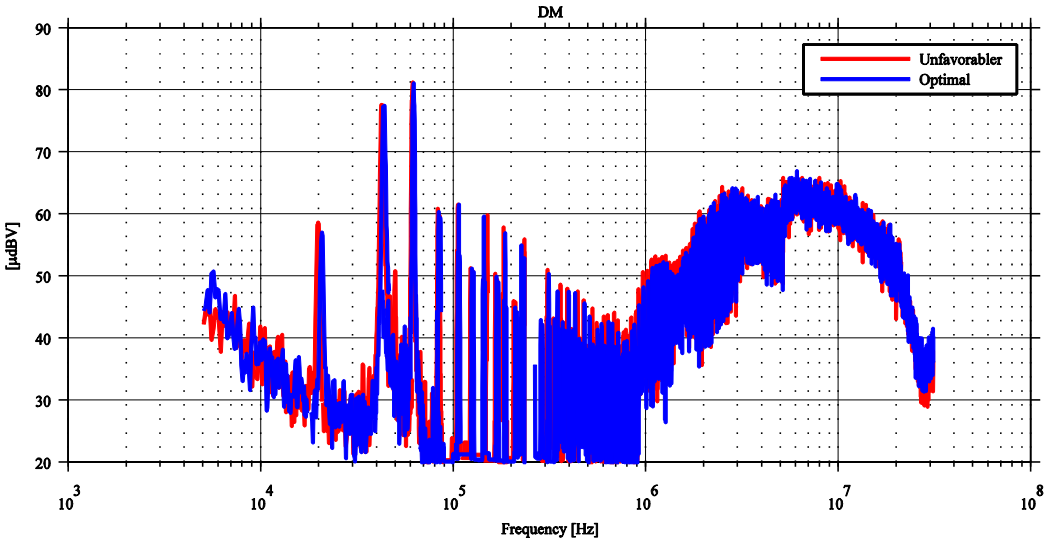

Fig. 3.15: The measured DM noise.

The DM noise is slightly reduced for the layout with the favorable capacitor placement in comparison to the layout with the unfavorable capacitor placement, especially for frequencies above $200kHz$. The measurement results and the simulations made in Maxwell agrees with [11] where it is stated that component placement affect the performance of a filter. Figure 3.16 shows that the CM noise at frequencies above $200kHz$ is not affected by component placements.

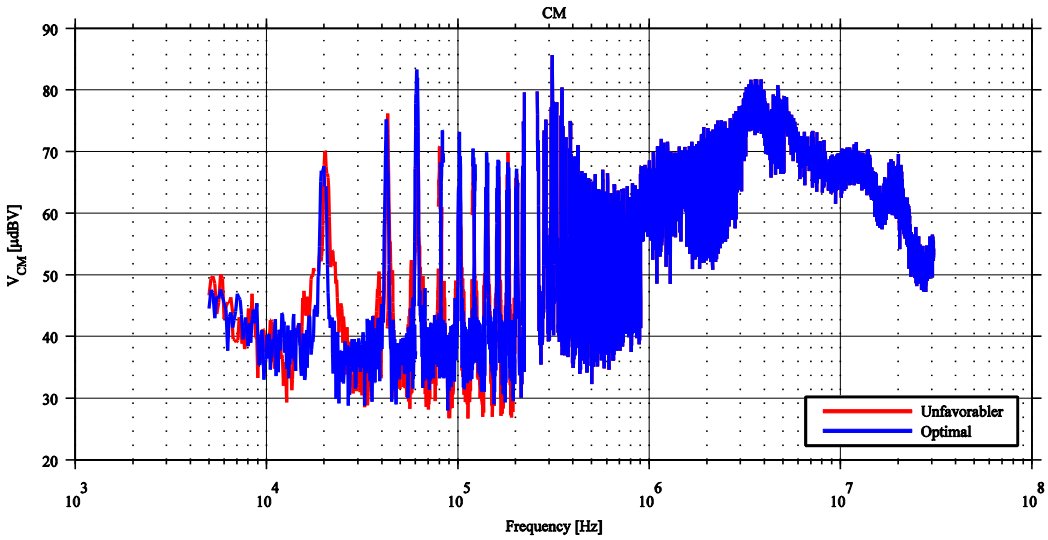

Fig. 3.16: The measured CM noise.

By favorable component placement the EMI levels of the inverter can be reduced but to find the cause of the EMI the simulation model needs to be extended and include more parts which in [1] was simplified and made ideal.

4 Improved Drive System Model

4.1 Improved PCB Model

The physical inverter PCB has four-layers where copper material is used as conductive material and FR4 epoxy as insulation material. The thickness of the conduction paths are $35\mu m$ and the thickness of the isolation layers are approximately $0.4mm$. The original design of the PCB is created in OrCad PCB Layout and the circuit layout is imported into Q3D Extractor. A cut-through section of the PCB can be seen in Figure 4.1 where the vias that connect each layer are included. The creation of vias and the positioning of each layer must be done manually.

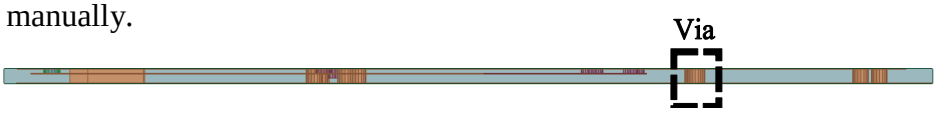

Fig. 4.1: A cut-through section of the four-layered PCB.

Due to the complex structure of the PCB, specific parts of the PCB model must be remodeled to reduce solution time. The model is simplified by removing the conduction paths that are connected to the driver circuit i.e., the only conduction paths included in the model are those that are connected to the main input voltage or ground. The conduction paths that have circular segments are simplified to obtain a coarser geometry. In Figure 4.2, all of the conduction paths of the PCB, except the ground planes and some vias are depicted.

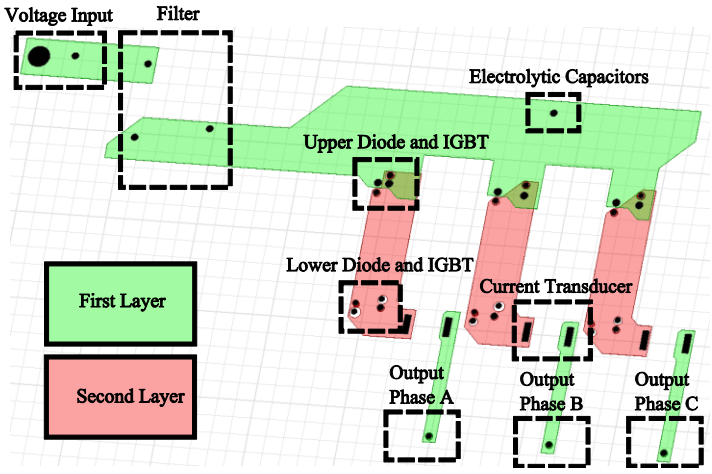

Fig. 4.2: Semi transparent top view of copper parts in the PCB constructed in Q3D.

The upper part the PCB trace in Figure 4.2 is connected to the main voltage input, filter and each phase leg. Connection points for the IGBTs and diodes are located at the first layer, which connects to the second layer by vias. The connection point to each electrolytic capacitor are simplified to one connection point. The groundplane is modeled as a copper sheet located beneath the PCB. The complete PCB model is shown in Figure 4.3.

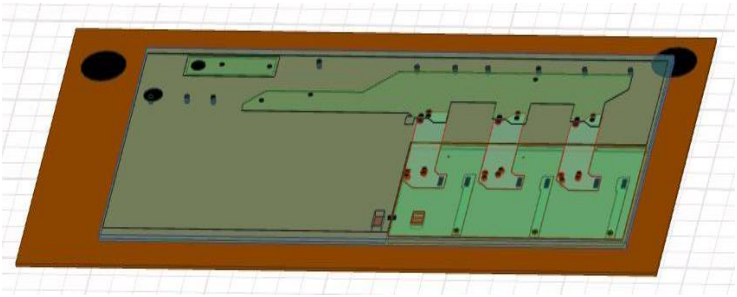

Fig. 4.3: Semi transparent top view of the complete PCB model.

In the simulation setup of the PCB model, the solution setup consists of a logarithmic interpolating sweep with four samples per decade from 0 to $30MHz$. The relative error is set to 0.5% and the maximum mesh refinement periods are 24. The results from Q3D Extractor are imported into Simplorer as a state space model. In Figure 4.4 and Table 4.1 , four parasitic capacitors of significant size from the solved PCB model are depicted at two frequencies.

Table 4.1: Four extracted parasitic capacitors from the PCB model.

Parasitic capacitor	Between nets	[pF] @ 0 Hz	[pF] @ 10 MHz
C_1	Ground One and protective earth ground.	44	44
C_2	Phase leg and Ground Two.	25	25
C_3	Phase leg and Ground One.	110	99
C_4	High voltage input and Ground One.	1100	1100

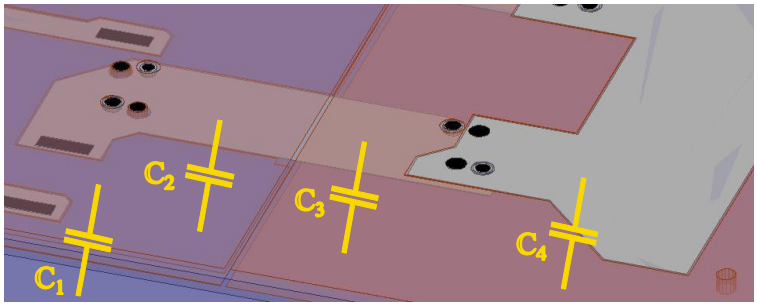

Fig. 4.4: View of PCB with significant parasitic capacitors indicated.

The imported model of the inverter is represented as a square shaped component where all the defined sources and sinks from Q3D Extractor are available as connection pins in Simplorer, see Figure 4.5.

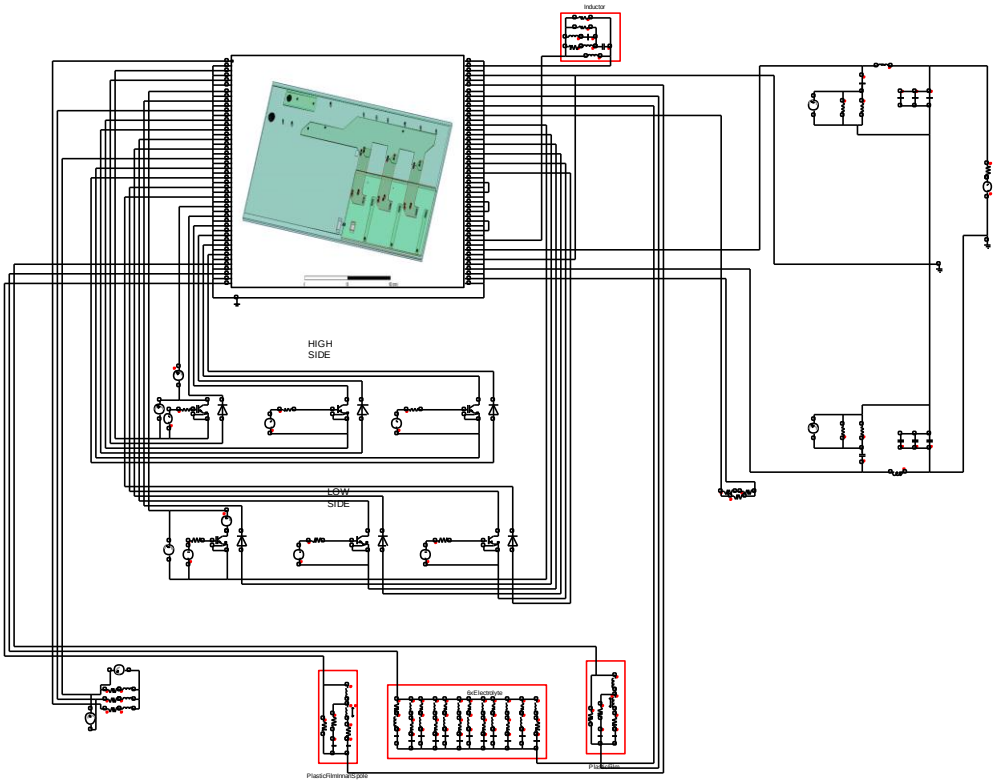

Fig. 4.5: Simplorer model with added PCB model

4.2 Improved Cable Model

The interconnecting cables between the inverter and the asynchronous motor needs to be more accurately modeled, and is modeled in the same manner as the PCB with Q3D Extractor. The original cable model is close to ideal since it has no parasitic components. Q3D Extractor will calculate the self resistance and the self inductance of each cable as well as the capacitive coupling between the cables to ground and between each cable. The cable model consists of three parallel isolated conductors, placed in a triangular manner, see Figure 4.6. The cable bundle is further placed on a copper sheet which serves as a ground plane. The dimension of the conductors, isolation and copper sheet used in the model are obtained by physical measurement. Accordingly, the radius of the conductor is $2.33mm$ where the radius of the isolation layer is $0.56mm$. The copper sheet is measured to $0.5mm$. Each power cable is assigned to a unique net containing a sink and a source. As with the PCB model, a copper sheet beneath the cables is also modeled and attached with a source and a sink.

Fig. 4.6: Bundle cable model.

The modeled cables are added as a static space state model in the existing Simplorer model in series with the motor model. By adding both a PCB model and a more accurate cable model the simulated EMI levels are increased which results in that the drive system model behaves more like the physical drive system, see Figure *4.7* and Figure 4.8.

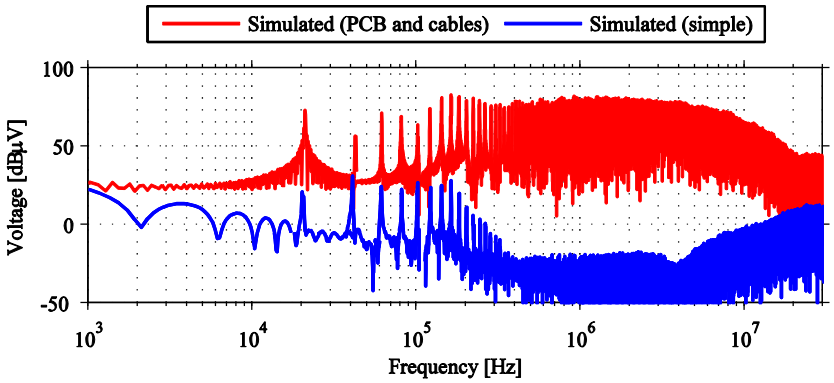

Fig. 4.7: Simulated EMI levels for the drive system model, with and without the addition of PCB and cables

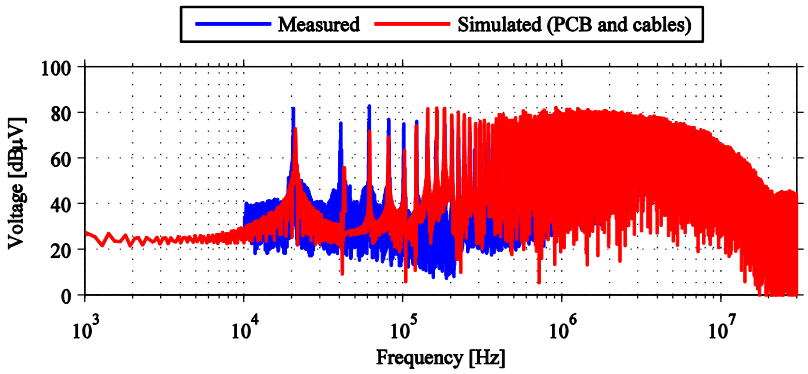

Fig. 4.8: EMI levels for model with added PCB and cables as well as measurements.

The instrument used for measuring the EMI is unable to accurately measure EMI levels in a large frequency span; it can only accurately measure a span of about $150kHz$ at a time which makes the measuring from $1MHz$ to $30MHz$ difficult. Because of this the EMI levels are measured just measured from $10kHz$ to $5MHz$ but with reduced accuracy above $1MHz$. By reducing the accuracy the measurements becomes "filtered" or averaged and it is therefore impossible to determine if the measurement results only consists of background noise or if it is EMI for higher frequencies. To study the content in the higher frequencies an accurate small range measurement is made from $10MHz$ to $10.05MHz$, i.e. the measuring span is $50kHz$. Figure 4.9 shows the accurate $10MHz$ measurement and an accurate measurements from $20kHz$ to $70kHz$.

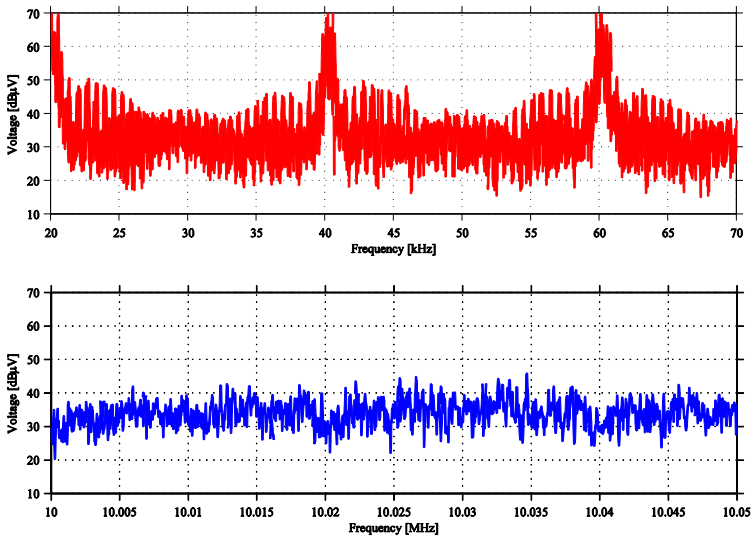

Fig. 4.9: Accurate EMI measurement. Upper: Low frequency, Lower: High frequency

The multiples of the switching frequency in Figure 4.9 should occur at $20kHz$, $40kHz$ and $60kHz$ which is clearly present. There should also be multiples of the switching frequency at $10MHz$, $10.02MHz$ and $10.04MHz$ but as seen in Figure 4.9 it is non existing as the measured EMI remains in the background noise level during the entire measured range. This shows that the simulation model is not accurate in the higher frequency range because in the simulated EMI level is high at $10MHz$, see Figure 4.8, which does not agree with the measurements.

5 Conclusion

To study the effects of inductive coupling, two EMI filter layout configurations were designed. The results indicate that the EMI levels are reduced if the plastic film capacitors have the short end facing the inductor core. In addition, the drive system in [1] has been extended with PCB and cable models. A difficult task in the modeling process was the simplifications which had to be made in order to obtain a solvable drive system model. A challenge in this field of work is to determine which specific components in the drive system that has a noticeable impact on EMI and which parts that can be neglected. Another difficult task in the modeling process is the definition of different references and grounds to be used in the drive system model. It has been shown, that this aspect is important since the CM noise component, which uses the ground plane as return path, is dominant in the high frequency range. The final result shows that it is possible to accurately model and simulate the EMI levels of an entire drive system. The EMI levels agree particularly well in the lower frequency range but for the higher frequency range additional improvements of the drive system model is required.

6 Future Work

More parts of the drive system can be more accurately modeled, for example the motor or the gate drive circuit. For the motor either a preconfigured template motor may be used in or a more detailed model of the motor can be designed in 3D where the physical dimensions as well as the material attributes of the motor are included. The CAD-model can then be implemented in FEM calculations to more accurately solve quantities such the magnetic flux and the produced torque. The gate drive circuit can be extended with additional parasitic components and a behavioral Spice-model provided by the manufacturer.

References

[1] E. Hallgren and M. Hedenskog, *Modeling and Validation of the EMI Performance of an Electric Drive System by Device Level Characterization*. Gothenburg: Chalmers University of Technology, 2011.

[2] J.-S. Lai, X. Huang, E. Pepa, S. Chen, and T. W. Nehl. (2006, Inverter EMI Modeling and Simulation Methodologies. *53(3)*, 736-744.

[3] H. Zhu, J.-S. Lai, A. R. Heffner, Y. Tang, and C. Chen. (2001, Modeling-Based Examination of Conducted EMI Emissions From Hard- and Soft-Switching PWM Inverters. *37(5)*, 1383-1393.

[4] H. Akagi and I. Matsumura, "Overvoltage mitigation of inverter-driven motors with long cables of different lengths," in *Energy Conversion Congress and Exposition (ECCE), 2010 IEEE*, 2010, pp. 862-869.

[5] C. R. Paul, *Introduction to Electromagnetic Compatibility*, 2 ed.: Wiley-Interscience, 2006.

[6] F. E. Terman, *Radio engineers' handbook*, 1. ed. ed. New York: McGraw-Hill, 1943.

[7] EMC Design Guide for Printed Circuit Boards: Ford Motor Company, 2002.

[8] S. Wang, "Modeling and Design of EMI Noise Separators for Multi-Phase Power Electronics Systems," *Power Electronics, IEEE Transactions on*, vol. PP, pp. 1-1, 2011.

[9] T. Williams, *EMC for product designers*. Oxford: Newnes, 2007.

[10] "Ansoft Q3D Extractor 10.02 User Manual," ed: Ansoft Corporation, 2010.

[11] A. Lissner, E. Hoene, B. Stube, and S. Guttowski, "Predicting the influence of placement of passive components on EMI behaviour," in *Power Electronics and Applications, 2007 European Conference on*, 2007, pp. 1-10.

[12] M. C. Caponet, F. Profumo, L. Ferraris, A. Bertoz, and D. Marzella, "Common and differential mode noise separation: comparison of two different approaches," in *Power Electronics Specialists Conference, 2001. PESC. 2001 IEEE 32nd Annual*, 2001, pp. 1383-1388 vol. 3.